HEAT TRANSFER ENHANCEMENT INSIDE CHANNEL BY USING THE LATTICE BOLTZMANN METHOD

by

Monireh ASADI ABCHOUYEH[a,b*], Mohammed EL GANAOUI[b], Rasul MOHEBBI[c], Mohammad Reza ZARRABI[a], Omid SOLAYMANI FARD[d], and Rachid BENNACER[e]

[a] School of Mathematics and Computer Science, Damghan University, Damghan, Iran
[b] Laboratoire Lermab-Longwy, University de Lorraine, IUT Henri Poincare de Longwy, Lorraine, France
[c] School of Engineering, Damghan University, Damghan, Iran
[d] Department of Applied Mathematics, Faculty of Mathematical Sciences, Ferdowsi University of Mashhad, Mashhad, Iran
[e] LMT/ENS-Cachan/CNRS/University Paris Saclay, Cachan, France

Original scientific paper
https://doi.org/10.2298/TSCI190919096A

In this study, the lattice Boltzmann method is employed in order to examine the fluid-flow and forced convection heat transfer inside a 2-D horizontal channel with and without obstacles. In order to enhance the heat and thermal energy transfer within the channel, different obstacle arrangements are posed to the flow field and heat transfer with the purpose of studying their sensitivity to these changes. The results indicate that, when the value of the Reynolds number is maximum, the maximum average Nusselt numbers happens on the lower wall (Case 4). The paper extends the topic to the use of nanofluids to introduce a possibility to enhancement of the heat transfer in the channel with an array of the obstacles with forced convection. For this purpose, the AgMgO-water micropolar hybrid nanofluid is used, and the volume fraction of the nanoparticle (50% Ag and 50% MgO by volume) is set between 0 and 0.02. The results showed that, when the hybrid nanofluid is used instead of a typical nanofluid, the rate of the heat transfer inside the channel increases, especially for the high values of the Reynolds number, and the volume fraction of the nanoparticles. Increasing the volume fraction of the nanoparticles increase the local Nusselt number (1.17-fold). It is shown that the type of obstacle arrangement and the specific nanofluid can exerts significant effects on the characteristics of the flow field and heat transfer in the channel. This study provides a platform for using the lattice Boltzmann method to examine fluid-flow through discrete obstacles in offset positions.

Key words: *lattice Boltzmann method, obstacle, forced convection heat transfer, nanofluid*

Introduction

Heat transfer has a wide range of applications in industry. Attention fluid-flow and forced convection heat transfer inside channels with obstacles is an important consideration in engineering applications such as thermal design of buildings, solar thermal collectors, *etc.* Increase in heat transfer with the purpose of improving the efficiency of heat exchanger devices can be achieved via different methods. Placing obstacles inside a channel is an appropriate

* Corresponding author, e-mail: m.asadi8689@gmail.com

method for this purpose, especially when the best locations and arrangements for the obstacles are found. A number of researchers have employed numerical and experimental techniques in order to study fluid-flow and heat transfer inside channels with obstacles.

For instance, Jubran *et al.* [1] placed both rectangular and square obstacles inside a channel in order to enhance its heat transfer. They reported that the individual rectangular modules caused a larger enhancement in the heat transfer inside the channel in comparison the square modules. The results of other studies have provided evidence that, as the space between obstacles is decreased, the fluid-flow in the channel is consequently enhanced, and that an increase in the Reynolds number, enhances the process of heat removal around the obstacles, chiefly around the obstacle corners [2-4]. In a numerical study, Mohamed Toumi *et al.* [5] investigated the 3-D shearing flows of Newtonian fluids around a cuboid obstacle. Their results showed that the locations after the obstacle and collision by the turbulent shearing flow generally formed a re-circulation area with a high concentration scalar. This means the area at the boundary-layer after the obstacle contained great turbulent energy. Kannan *et al.* [6] investigated the effects of different geometric obstacles and different values of the Reynolds number on the steady-state of the laminar flow in a staggered lid-driven cavity with a heated obstacle. The resultsindicated that, for all the different geometric obstacles, the drag coefficient decreased and the average Nusselt number increased when the value of the Reynolds number was expanded. Dubovsky and Letan [7] undertook a numerical and experimental study on the effects of an array of hollow obstacles formed on heated extended plates on the heat transfer in a rectangular channel in air forced convection. The results showed a notable increase in the heat transfer for the long plates.

The use of nanofluids constitutes another method for enhancing the output of thermal systems by raising the heat transfer inside the channel. Nanofluids are particles with sizes smaller than 100 nm, and they have much more thermal conductivities than base fluids [8, 9]. Nanofluids can be used in industrial cooling applications, solar devices*, etc.* The use of nanofluids as a coolant was introduced by Choi [10]. The most popular nanoparticles used in industrial applications are CuO, TiO_2, Al_2O_3, SiO_2, Al, and Cu (metal and metal-oxides). Using the LBM, Yuan *et al.* [11] employed different parameters (*i.e.*, Reynolds number, vertical passage ratio, and nanoparticle solid volume fractions) in order to examine the effects of different nanofluids on the forced convection heat transfer inside a channel with obstacles attached to the up and bottom walls. They concluded that the local and average Nusselt numbers would increase by increasing the value of the Reynolds number and decreasing the value of the vertical passage ratio. In order to obtain the optimal nanofluid heat transfer, Boulahia *et al.* [12] conducted a numerical study on the heat transfer in a square cavity with inside circular heating and cooling bodies. The results showed that the optimal heat transfer could be achieved when the circular body was placed near the bottom wall of the cavity. Athinarayan *et al.* [13] carried out a numerical study on the forced convection heat transfer of nanofluids over a square cylinder placed in a confined channel. They reported that two vortices with different sizes were formed behind the cylinder. The size of smaller vortex expanded linearly when the values of the Reynolds number and volume fraction were increased. In addition, the value of the local Nusselt number increased once the nanoparticles were incorporated into the base fluid.

Nanoparticles have a great potential to enhance the process of heat transfer, especially if more than one type of nanostructure are combined in a Nanoassembly. It is predictable that the combination of two or more nanoparticles can increase heat transfer. Hybrid nanoparticles can be defined as two or more different materials with a nanometer size [14, 15]. The use of hybrid

nanofluids in industry is a relatively new idea, which has been generally accepted in the last decade. In recent years, hybrid models are widely used in various heat transfer applications such as micro-channels, air conditioning systems, coiled heat exchangers*, etc.* Wang *et al.* [16] mixed CuO and Al_2O_3 nanoparticles with water as a base fluid for the first time. They observed that the nanoparticle-fluid mixture had a more thermal conductivity than the nanofluid alone. Mollamahdi *et al.* [17] used the analytical least square method and the numerical fourth order Rung-Kutta method in order to investigate the effects of a micropolar hybrid nanofluid (MgO-Ag-water) on the heat transfer in a permeable channel. They demonstrated that the heat transfer increased when the hybrid nanofluid was used instead of a simple nanofluid. More research on the effects of hybrid nanofluids on the process of heat transfer can be found in [18-27].

The lattice Boltzmann method (LBM) is a flexible and powerful numerical method introduced in the 1980. It easily responds to complex geometries and is able to perform complicated parallel computations [28-32], making it a powerful tool of fluid simulation for understanding important processes related to heat transfer. Lately, the LBM has been favored over the competing methods for simulating nanofluid heat transfer [33]. Using the LBM coupled with a finite difference, Boutra *et al.* [30] numerically analyzed the hydrodynamic and thermal characteristics of an Ag-water nanofluid in a cubical enclosure. In their enclosure, there existed a heated source located in the center of the bottom wall. The results showed that the process of the heat transfer in the enclosure would be enhanced by increasing the volume fraction of the nanoparticles, the value of the Rayleigh number, and the width and height of the bottom heat source. Mohebbi *et al.* [34] utilized the LBM in order to examine the effects of the presence of one sinusoidal obstacle and four sinusoidal side obstacles in difference order [35] on the nanofluid natural and forced convection in the channel. They observed that, for all the sinusoidal obstacles and different values of the Reynolds number, the process of heat transfer was enhanced by raising the volume fractions of the nanoparticles, and that the average Nusselt number increased as a result of the decrease in the amplitude of the wavy wall of the sinusoidal obstacles and the space between the obstacles.

The novelty of this paperresides in the fact that the study employs the LBM in order to examine the impacts of the existence and order of the obstacles in the channel on the fluid-flow and heat transfer in the presence of the Ag-Mgo-water micropolar hybrid nanofluid and absence of nanoparticles.

Definition of the case test region

The computational domain considered in this study includes a channel with the length, L, and with and without an array of obstacles at the constant temperature $T_c = 0$, height b, and length a, $a/b = 1$ and $a/L = 0.015$, which are located inside the channel at the temperature $T_{in} = 0$, fig. 1. The top and bottom of channel walls are kept at $T_w = 1$. Five different cases are identified based on the location (as $\bar{x} = x/L$), and shape (0 for rectangular, 1 for zigzag) of the obstacle array; *i.e.*, Case 1: $'\bar{x} = 0.26, 0'$, Case 2: $'\bar{x} = 0.26, 1'$, Case 3: $'\bar{x} = 0.2, 1'$,

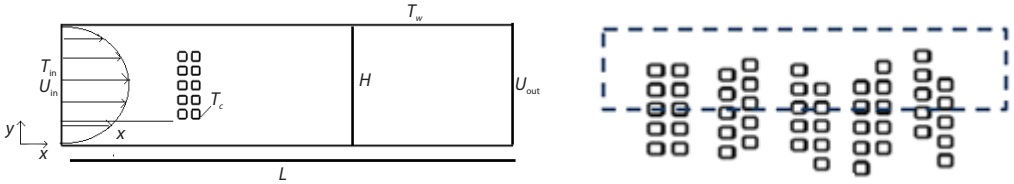

Figure 1. Specifications of the computational domain and obstacles position

Case 4: $'\overline{x}$ = 0.2, 1′, and Case 5: $'\overline{x}$ = 0.2, 1′. In fig. 1, H indicates the height of the channel, and x represents the distance of the first obstacle from the entrance of the channel. The fluid with the parabolic velocity enters the channel with the width $\overline{H} = H/L = 0.25$. The Reynolds number range between 40 and 100 and the solid volume fractions of the nanoparticles range between 0 and 0.02. The thermo physical properties of the basic fluid and nanoparticles are summarized in tab. 1.

Table 1. Thermophysical properties of the base fluid and nanoparticles

Property	Water	MgO	Ag
ρ [kgm^{-3}]	997.1	3560	10500
c_p [Jkg^{-1}K^{-1}]	4179	955	235
k [Wm^{-1}K^{-1}]	0.613	45	429

Computational method and simulations

The LBM is an increasingly employed simulationol founded and extended by Frisch *et al.* [36, 37] based on a statistical idea. This method is used to simulate fluid-flow and heat transfer in complex geometries [38]. Compared to the classical macroscopic Navier-Stokes (NS) method, the LBM adopts a mesoscopic approach in which the fluid field is composed of a group of microscopic particles represented by a velocity distribution function. Due to its kinetic nature, the LBM is capable of simulating porous media flows, flows of suspensions, and compressible flows, the LBM draws on the motion of liquid particles in order to calculate macroscopic quantities such as speed, pressure, and temperature. The purpose of this method is to break the fluid domain into Cartesian cells. Based on the number of the moving liquid particles, a fixed number of distribution functions is then assigned to each cell. In this study the D_2Q_9 model of the LBM used. In this model, there are nine sets of particles with different velocities in every lattice.

Two steps are taken in order to run the LBM: collision and streaming. The general form of the LBE, known as the BGK (Bhatnagar, Gross, and Crook) equation, can be expressed [38]:

$$f_i\left(\boldsymbol{x}+\boldsymbol{e_i}\Delta t, t+\Delta t\right)-f_i\left(\boldsymbol{x},t\right)=\frac{1}{\tau_f}\left(f_i-f_i^{\mathrm{eq}}\right) \tag{1}$$

where f_i is the distribution function, e_i – the finite set of the discrete velocities (depending on the dimension and number of the velocity directions) in the direction i, Δt – the lattice time step, τ_f – the single relaxation time of the fluid, and f_i^{eq} – the local equilibrium distribution function:

$$f_i^{\mathrm{eq}}=\rho\omega_i\left[1+\frac{3\boldsymbol{e_i}\boldsymbol{u}}{c^2}+\frac{9}{2}\frac{\left(\boldsymbol{e_i}\boldsymbol{u}\right)^2}{c^4}-\frac{3}{2}\frac{\boldsymbol{u}^2}{c^2}\right] \tag{2}$$

where $\boldsymbol{u}$ and ρ are the macroscopic velocity vector and density, respectively, and ω_i is the weight, which has the values of $\omega_0 = 4/9$, $\omega_1 = 1/9$, for i = 1-4, and $\omega_i = 1/36$ for i = 5-8. The discrete velocity $\boldsymbol{e_i}$ is defined:

$$\boldsymbol{e_i}=\left\{\cos\left[\pi/2\left(i-1\right)\right],\sin\pi/2\left[\left(i-1\right)\right]\right\}c,\ \text{for}\ i=1\text{-}4$$

$$\boldsymbol{e_i}=\sqrt{2}\left\{\cos\left[\left(i-5\right)\pi/2+\pi/4\right],\sin\left[\left(i-5\right)\pi/2+\pi/4\right]\right\}c,\ \text{for}\ i=5\text{-}8\ \text{and}\ \boldsymbol{e}_0=0$$

The macroscopic quantities such as density, ρ, and the velocity, $\boldsymbol{u}$, are available through the distribution functions as $\rho = \sum_0^8 f_i$ and $\rho = \sum_0^8 e_i f_i$.

For the temperature field, the thermal LBM employs the distribution function g:

$$g_i\left(\boldsymbol{x}+\boldsymbol{e_i}\Delta t, t+\Delta t\right)-g_i\left(x,t\right)=-\frac{1}{\tau_g}\left(g_i-g_i^{\mathrm{eq}}\right) \tag{3}$$

where the equilibrium temperature distribution function, g_i^{eq}, is computed:

$$g_i^{\mathrm{eq}}=\omega_i T\left[1+\frac{\boldsymbol{e_i u}}{c^2}\right] \tag{4}$$

where c is the lattice speed. The macroscopic temperature quantity is given:

$$T=\sum_0^8 g_i \tag{5}$$

Due to the importance of optimal energy consumption in industrial applications such as heat exchangers, the increment heat transfer needs to be considered in these applications. The poor thermal conductivity of fluids puts a major limit on the process of heat transfer. By adding nanoparticles to a base liquid, a combination is obtained that exerts a significant increase on heat transfer and changes the thermo physical properties of the base fluid such as its thermal conductivity, thermal diffusivity, viscosity, and convective heat transfer coefficients. In simulation of nanofluids via the LBM, nanofluids would act differently from pure liquids as a result the forces on nanoparticles. The characteristics of the nanofluid used in this study, *i.e.*, its density, effective dynamic viscosity, diffusion coefficient, and heat capacity [39, 40], are, respectively defined as:

$$\rho_{\mathrm{nf}}=\left(1-\varphi\right)\rho_{\mathrm{f}}+\frac{\varphi}{2}\rho_{\mathrm{pAg}}+\frac{\varphi}{2}\rho_{\mathrm{pMgO}} \tag{6}$$

$$\mu_{\mathrm{nf}}=\left(1+32.79\varphi-721\varphi^2+714600\varphi^3-0.1941\cdot 10^8\varphi^4\right)\mu_{\mathrm{f}} \tag{7}$$

$$\alpha_{\mathrm{nf}}=\frac{k_{\mathrm{nf}}}{\left(\rho c_p\right)_{\mathrm{nf}}} \tag{8}$$

$$\left(\rho c_p\right)_{\mathrm{nf}}=\left(1-\varphi\right)\left(\rho c_p\right)_f+\frac{\varphi}{2}\left(\rho c_p\right)_{\mathrm{pAg}}+\frac{\varphi}{2}\left(\rho c_p\right)_{\mathrm{pMgO}} \tag{9}$$

where φ is the solid volume fraction and subscripts f, p, and nf refer to basefluid, nanoparticle, and nanofluid, respectively. Thermal conductivity of the nanofluid can be approximated through:

$$k_{\mathrm{nf}}=\left(\frac{0.1747\cdot 10^5+\varphi}{0.1747\cdot 10^5-0.1498\cdot 10^6\varphi+0.1117\cdot 10^7\varphi^2+0.1997\cdot 10^8\varphi^3}\right)k_{\mathrm{f}} \tag{10}$$

where k_{f} is the thermal conductivities of the pure water.

Boundary conditions

Zou and He [41] model is used in order to set the boundary conditions, and an extrapolation method is employed in order to simulate the inlet and outlet flow. Also, the standard Bounce-Back boundary conditions are employed for the boundaries of the solid walls. By using Mohamad's [42] method, the temperature of the inlet fluid is set to zero, $T_{\mathrm{in}}=0$, and the other walls are set at a fixed temperature, $T_{\mathrm{w}}=1$.

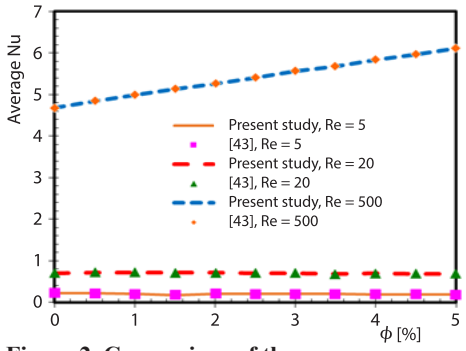

Figure 2. Comparison of the average Nusselt numbers for the different volume fractions of thenanoparticles, the present study *vs.* [43]

Table 2. Results of the grid independence test for Re = 100

Number of nodes	Average Nusselt number
801 × 801	14.3125
1601 × 1601	18.8432
3201 × 3201	18.8970

Code validation and method accuracy

In order to validate the numerical results of the LB simulation run in the present study, a comparison is made between these results and those obtained in Santra *et al*. [43]. As seen in fig. 2, there is a good agreement between the two sets of results. Grid independency for the code is shown in tab. 2. Grids ranging from 801-3201 are examined and an intermediate grid of 1601 is selected to provide good agreement between accuracy and computing time of the method for the simulated cases.

Results and discussion

The effects of the obstacle presence on the channel

This study examines the effects of the presence or absence of obstacles and their arrangement variations on the fluid-flow and heat transfer in a 2-D horizontal channel. An incompressible Newtonian laminar fluid is selected for flow through a long channel of constant cross-section. The results and figures in this paper concern only a limited number of the examined cases, presented to exemplify their relative features and characteristics. For all the cases at the inlet, a uniform velocity profile is produced.

Figure 3 shows the variation in the velocity and temperature inside the channel without any obstacle for Re = 40. The figure indicates that there is no change in the flow, and that the distribution of the temperature is uniform.

Figure 4 shows the variations of the velocity inside the channel for Re = 40 and 100 in Case 1. The figure indicates that, for all the values of the Reynolds number, once the developed fluid-flow enters the channel, it reaches the first obstacles diverted from the straight path and moves to the top and bottom walls, which leads to enhancing the heat transfer rate. In this case, two high velocity regions are created between the walls and the first row of the obstacles. The maximum velocity is enhanced by increasing the value of the Reynolds number. It is also observed that some low velocity zones are formed between the obstacles due to boundary-layer separation. For the lower values of the Reynolds number, the region of the flow field in which the viscosity effects are significant is smaller than the region of the higher Reynolds number, by increasing the value of Reynolds number, the effects of the fluid inertia become more important. By comparison between figs. 3(a) and 4 it can be found that, when there is no obstacle inside the channel, no change happens in the velocity profile, and therefore, no increase is observed in the heat transfer in the channel. In Case 1, the viscosity effects are observed throughout a relatively large area of the flow field due to the presence of the obstacles.

Figure 5 represents the isotherms contours plotted for the different values of the Reynolds number in Case 1. It is seen from the figure that the isotherm contours near the walls of the

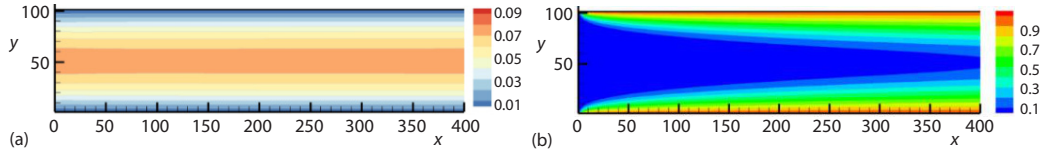

Figure 3. Variation in (a) the velocity and (b) the temperature inside the channel for Re = 40

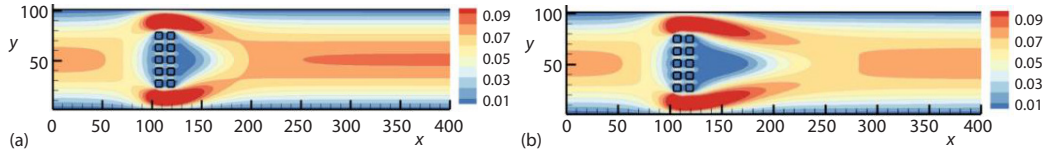

Figure 4. Variation in the velocity inside the channel for Case 1 *vs.* (a) Re = 40 and (b) Re = 100

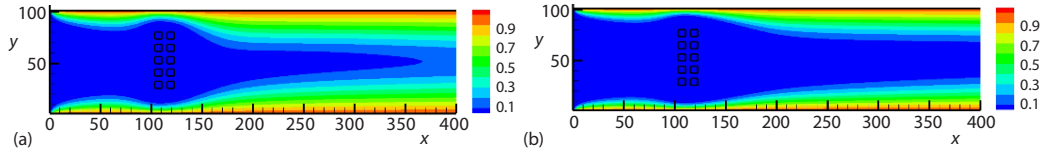

Figure 5. Variation in the temperature inside the channel for Case 1 *vs.* (a) Re = 40 and (b) Re = 100

channel in the block zone are more compact and that the thermal expanding length grows and approaches the walls as the value of the Reynolds number is increased. In other words, the isotherm contours become denser with increases in the Reynolds number. It can be concluded that the effects of the temperature gradient on the walls of the channel become more considerable as the value of the Reynolds is enhanced, which in return increases the rate of the heat transfer. For Case1, the changes in the local Nusselt number corresponding to the different values of the Reynolds are also investigated (not shown here). The local Nusselt number reaches its highest value at the entry to the channel, and its value reduces along the channel. Due to the high temperature gradient, the value of the local Nusselt number varies very sharply near the obstacles over the wall of the channel. The value subsequently decreases after the obstacles as a result of the flow leaving the boundary-layer for redistribution as Poiseuille flow, leading to a decrease in the rate of the heat transfer. In this case, the values of the local Nusselt number for the two walls are found to be the same. Where there is no obstacle in the channel, the value of the local Nusselt number decreases sharply, and then, the value becomes fixed. With the obstacles located in the channel, a keen point is observed on the curve of the distribution of the local Nusselt number, which is due to the encounters of the fluid-flow with the obstacles.

The effects of the changes in the obstacles arrangement on the heat transfer

In this section, numerical analysis is employed to compare the convective heat transfer behaviors in the channel with respect to some arrangements of the obstacles. Some observed changes are examined against the obstacle locations and their effects on the heat transfer inside the channel. In Case 2, the first column is fixed while the second column is moved upwards as far as an obstacle. In Case 3, the second column is fixed while the first column is moved upwards as far as two obstacles. In Case 4, both columns are moved as far as an obstacle whereby the first column is moved down and the second column is moved up. In Case 5, both columns are moved as far as an obstacle whereby the first column is moved up and the second column is moved down, fig. 6(a).

Figure 6(b) shows the effect of the different cases on the streamlines for Re = 100 and $\phi = 0.00$. The streamlines near the front face of the obstacles leave the obstacles and pass around a recirculating wake. Near the obstacles, the flow suddenly shrinks and diverts at the upstream and downstream corners of the obstacles in all the cases. In Cases 3-5, due to the arrangement

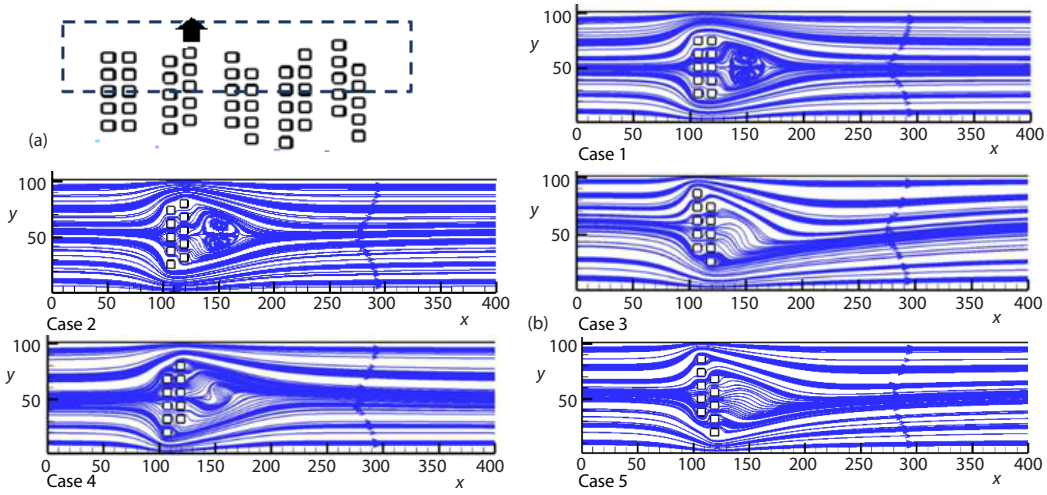

Figure 6. The changes in the obstacle arrangement; (a) variation in the streamlines inside the channel for Re = 100 and (b) $\phi = 0.00$ for the different cases

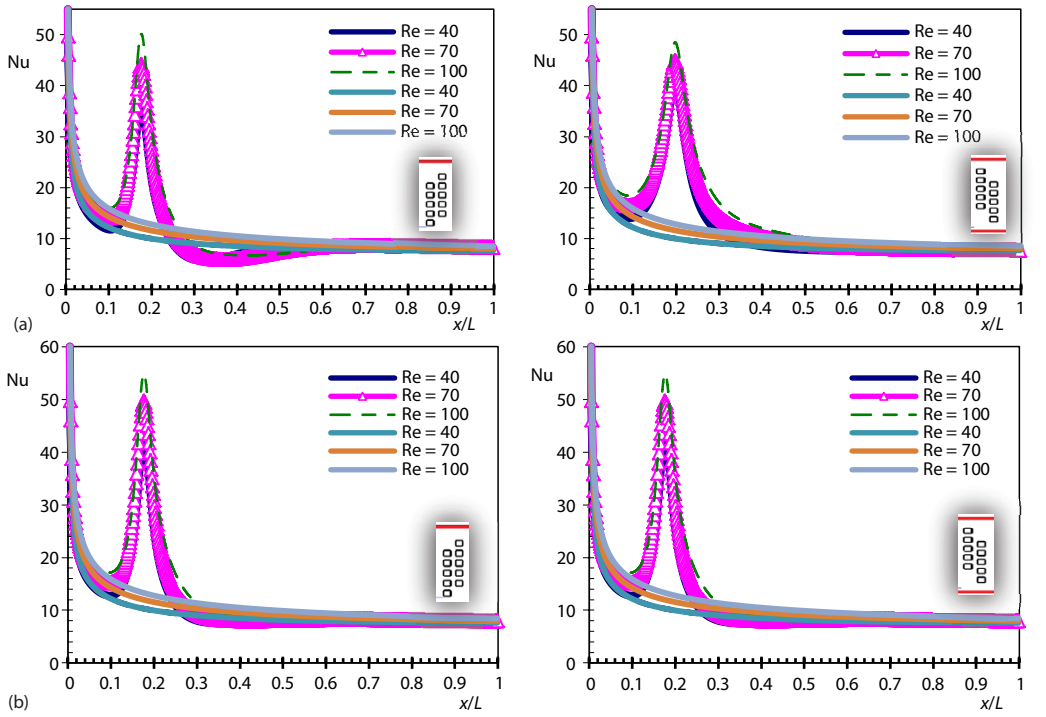

Figure 7. The local Nusselt number for the various values of the Re at $\phi = 0.0$ in Cases 4 and 5 on (a) the lower wall and (b) the upper wall

of the obstacles, the streamlines pass through the obstacles with a temporal delay from each other, and the flow continues to move without forming any vortex. Nevertheless, in the two other Cases (1 and 2), the streamlines pass through the obstacles simultaneously, and as a result of the sudden expansion in the cross-section, two vortices are formed behind the obstacles, after which the flow reattachment is established.

Figure 7 represents the changes in the value of the local Nusselt number over the walls of the channel for the different values of the Reynolds number at $\phi = 0.00$ in Cases 4 and 5. The value of the local Nusselt number over the two walls are almost the same. The heat transfer between the fluid and obstacles on the upper wall is somehow better than that on the down wall.

Table 3 presents the compression results of the heat transfer in the channel on the lower and upper walls for Re = 100 and $\phi = 0$. The results for the channel without the obstacles are considered as the point of reference, based on which the changes in the average and local Nusselt number and the percentage increase in the heat transfer are presented (the local Nusselt number for the lower and upper wall of channel without obstacles are 11.259 and 11.253, respectively). As seen from tab. 3, the maximum enhancement in the heat transfer on the lower and upper wall happens in Cases 4 and 3, respectively. In fact, these two cases are symmetric and moving obstacles up or down leads to equal results due to the symmetric arrangements of obstacles.

In tab. 4, the pressure drops across the channel for Re = 100 with respect to all the cases are summarized. As one can see from the table, the highest pressure drop happens in Case 5. It is clear that the presence of the obstacles in the channel causes resistance to the flow and leads to the pressure drop.

Table 3. The compression results of heat transfer for Re = 100 and $\phi = 0$ on upper and lower wall

	Lower wall			Upper wall		
Cases	Average Nusselt number	Maximum local Nusselt number	Enhancement [%]	Average Nusselt number	Maximum local Nusselt number	Enhancement [%]
Case 1	13.119	35.8	14.177	13.125	37.5	14.263
Case 2	13.477	39.2	16.527	12.996	39.0	13.41
Case 3	13.141	46.3	14.32	14.10	42.3	17.924
Case 4	14.220	39.7	20.82	12.062	49.8	6.7093
Case 5	14.156	48.0	20.41	12.992	54.6	13.384

Table 4. The pressure drop across the channel for Re = 100

Cases	$p_{out} - p_{in}$
Case 1	10.4874
Case 2	12.0011
Case 3	14.9990
Case 4	14.8803
Case 5	19.9034
Without obstacle	1.9469

The effects of the nanofluid on the heat transfer

Because of the random motion of the nanoparticles, a higher thermal conductivity is observed in the nanofluids compared to that in the fluids. This higher thermal conductivity depends on the parameters of the nanoparticles including size, volume fraction, aspect ratio, thermo physical properties of the base fluid, and temperature. Bennacer *et al.* [44] investigated fluid the flow and heat transfer inside a cavity with nanoparticles and presented a mathematical model as a result. They proposed an empirical formula to predict the rate of heat transfer whereby heat transfer was defined as a function of nanoparticle concentration. Also, they concluded that, due to the nature of natural-convection, remarkable increase in heat transfer would not happen for particle concentration. This section focuses on the effects of the nanofluid on the fluid-flow and heat transfer inside the channel as observed in the present study.

Figure 8 indicates the isotherms contours plotted for Re = 40 for the different values of the volume fraction of the nanofluid in Cases 2 and 4. In this figure, the effects of using the hybrid nanoparticles on the temperature inside the channel are depicted. The figure shows that using the hybrid nanoparticles increases the temperature of the channel. Also, it is seen that the isotherm contours are thin near to the wall of the channel in the obstacle area, and that the thermal boundary-layer thickness (TBLT) decreases in this region.

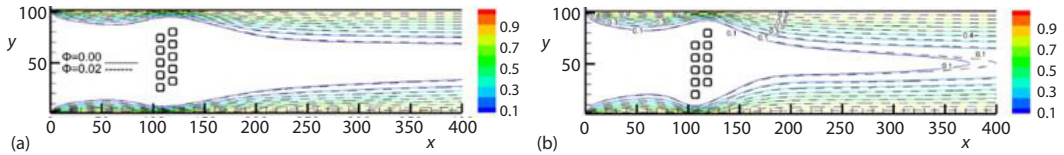

Figure 8. Variation in the temperature inside the channel for Re = 40 in Cases 2 and 4 for the different values of the volume fraction of the nanofluid

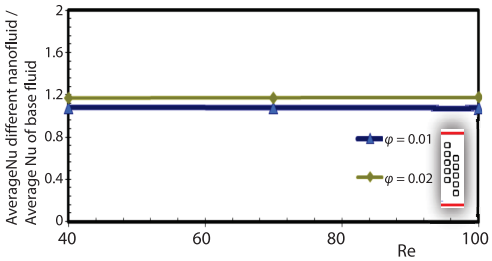

Figure 9. Variations of nanofluid-to-water ratio of average heat transfer coefficient with particle volume concentration for different values of particle volume concentration, present numerical results Case 5

Figure 9 shows the numerical prediction for the nanofluid-to-water ratio of average convective heat transfer coefficients *vs.* Reynolds number at various particle volume concentration. As one can see, the use of nanofluids increases the average heat transfer coefficient. Also, it is found that the average heat transfer coefficient increases with particle volume concentration for a fixed Reynolds number.

Conclusion

Examining the fluid-flow in channels helps understand the related physical phenomena and to test the validity of the new computational approaches before generalizing any situation complex coupled physics and realistic situations in industry (*e.g.*, reactive flows, bubbles, cooling, *etc*.). In the present study, the effects of different obstacle arrangements on the fluid-flow and forced convection heat transfer in a 2-D channel was investigated via the LBM. For this purpose, the AgMgO-water micropolar hybrid nanofluid is used, and the volume fraction of the nanoparticle (50% Ag and 50% MgO by volume) is set between 0 and 0.02. Different values of the Reynolds numbers and solid volume fraction are set in order to show how the obstacle arrangements with various characteristics can have effects on the flow dynamics and heat transfer enhancement in the channel. The results indicate that the obstacle arrangement has

a significant effect on the isotherms, streamlines, and total heat transfer in the channel. These results support the conclusion that the process of heat transfer is enhanced as a result of the high values of the Reynolds number. In the present study, the traditional belief about the minor effects of nanofluids in heat transfer is also supported by the results of the LBM. These findings provide the basis for extending the use of the LBM to other issues related to complex physics.

By Comparison between values of the local Nusselt number it cab be found that, increase in the value of the volume fraction of the nanoparticles from 0 to 0.02 in all the five cases results in a 1.17-fold in the value of the local Nusselt number in the corners of the upper and lower walls of the channel. The maximum enhancement in the heat transfer on the lower and upper wall happens in Cases 4 and 3, respectively. In fact, these two cases are symmetric and moving obstacles up or down leads to equal results due to the symmetric arrangements of obstacles. The maximum value of the average Nusselt belongs to Case 4, happening on the lower wall of the channel for Re = 100 and $\phi = 0.02$ (16.69853). In this case (Case 4), the maximum difference in the average Nusselt number between the lower and upper wall of the channel is found to be 2.53454. The results indicate that the increase in the local Nusselt number is greater in the cases that both columns are displaced and also the highest increase is when the first column shifts.

This study is the first attempt to use the LBM to study fluid-flow through discrete obstacles in offset positions. The study is intended to model the effects of a tilt angle and isothermal obstacles in increasing heat transfer with the purpose of increasing our understanding of thermo-fluidic phenomena by using the capacities of the LBM, which can take complex boundary conditions into account and provide results under reasonable computational time.

Acknowledgment

The first author thanks the IUT of Longwy, the Energy research Lab, at University of Lorraine and University of Paris-Saclay for their support for making this research possible.

Nomenclature

c – lattice speed
c_p – specific heat, [Jkg^{-1}K^{-1}]
g – energy distribution function,
H – channel's height, [m]
h – obstacle's height, [m]
h – heat transfer coefficient, [Wm^{-2}K^{-1}]
k – thermal conductivity, [Wm^{-1}K^{-1}]
L – length of the channel, [m]
Nu – local Nusselt number (= hL/k)
Pr – Prandtl number (= ν/α)
Re – Reynolds number (=UD/ν)
T – temperature, [K]
u, v – velocity components, [ms^{-1}]
$\boldsymbol{u}$ – velocity vector, [ms^{-1}]

Greek symbols

μ – dynamic viscosity, [kgm^{-1}s^{-1}]
δ_x, δ_y – lattice spacing
δ_t – time step
ν – kinematic viscosity, [m^{2}s^{-1}]
ω – weight function

Subscripts

f – fluid
i – move direction of single-particle
nf – nanofluid
p – particle

References

[1] Jubran, B. A., *et al*., Convective Heat Transfer and Pressure Drop Characteristics of Various Array Configurations to Simulate the Cooling of Electronic Modules, *International Journal of Heat and Mass Transfer*, *39* (1996), 16, pp. 3519-3529
[2] Korichi. A., *et al*., Numerical Heat Transfer in a Rectangular Channel with Mounted Obstacles on Upper and Lower Walls, *International Journal of Thermal Sciences*, *44* (2005), 7, pp. 644-655
[3] Pirouz, M. M., *et al*., Lattice Boltzmann Simulation of Conjugate Heat Transfer in a Rectangular Channel with Wall-Mounted Obstacles, *Scientia Iranica*, *18* (2011), 2, pp. 213-221

[4] Gareh, S., Numerical Heat Transfer in a Rectangular Channel with Mounted Obstacle, *International Letters of Chemistry, Physics and Astronomy*, *19* (2014), 2, pp. 111-119
[5] Toumi1, M., *et al*., The 3-D Study of Parallel Shear Fow Around an Obstacle in Water Channel and Air Tunnel, *Mechanics & Industry*, *18* (2017), 505, 13
[6] Kanna, M. S., *et al*., Investigation of Forced Convection Heat Transfer from a Block Located Staggered Cavity with Parallel and Anti-Parallel Wall Motion, *Thermal Science*, *23* (2019), Suppl. 4, pp. S1281-S1380
[7] Dubovsky, V., Letan., R., Air Forced Convection over Two-Side Plate Extended by Rectangular Hollow Blocks, *Thermal Science*, *23* (2019), Suppl. 4, pp. S1251-S1260
[8] Sahid, N. S. M., *et al*., Neural Network Modelling of Grinding Parameters of Ductile Cast Iron Using Minimum Quantity Lubrication, *International Journal of Automotive and Mechanical Engineering*, *1* (2015), 11, pp. 2608-2621
[9] Najiha, M. S., Rahman, M. M., Experimental Study on Minimum Quantity Lubrication in end Milling of AA6061-T6 Using Tialn Coated Carbide Tools, *International Journal of Automotive and Mechanical Engineering*, *1* (2015), 11. pp. 2771-2785
[10] Choi, S., Developments and Applications of Non-Newtonian Flows, *American Society of Mechanical Engineers*, *66* (1995), Nov., pp. 99-105
[11] Yuan, M., *et al*., Study of Nanofluid Forced Convection Heat Transfer in a Bent Channel by Means of Lattice Boltzmann Method, *International Journal of Heat and Mass Transfer*, *30* (2018), 3, pp. 1291-1303
[12] Boulahia. Z., *et al*., Numerical Study of Natural and Mixed Convection in a Square Cavity Filled by a Cu-Water Nanofluid with Circular Heating and Cooling Cylinders, *Mechanics & Industry*, *18* (2017), 502, pp. 21-32
[13] Athinarayan, A., *et al*., Numerical Investigation of Heat Transfer from Flow over Square Cylinder Placed in a Confined Channel Using Cu-Water Nanofluid, *Thermal Science*, *23* (2019), Suppl. 4, pp. S1367-S1380
[14] Syam Sundar. L., et al., Investigation of Thermal Conductivity and Viscosity of Fe_3O_4 Nanofluid for Heat Transfer Applications, *International Communications in Heat and Mass Transfer*, *44* (2013), May, pp. 7-14
[15] Leong, K. Y., *et al*., Synthesis and Thermal Conductivity Characteristic of Hybrid Nanofluids, *Renewable and Sustainable Energy Reviwes*, *75* (2017), Aug., pp. 868-878
[16] Wang, X., *et al*, Thermal Conductivity of Nanoparticle-Fluid Mixture, *Journal Thermophys Heat Transfer*, *13* (1999), 4, pp. 474-480
[17] Mollamahdi, M., *et al*., Flow Field and Heat Transfer of *MgO-Ag/Water Micropolar Hybrid Nanofluid in a Permeable Channel,* Trans. Phenom. NanoMicro Scales, *6* (2018), 1, pp. 13-26
[18] Ho, C. J., *et al*., Preparation and Properties of Hybrid Water-Based Suspension of Al_2O_3 Nanoparticles and MEPCM Particles as Functional Forced Convection Fluid, *International Communications in Heat and Mass Transfer*, *37* (2010), 5, pp. 490-494
[19] Suresh, S., *et al*., Synthesis of Al_2O_3-Cu/Water Hybrid Nanofluids Using Two Step Method and Its Thermo Physical Properties, Colloids and Surfaces A: *Physicochemical and Engineering Aspects*, *388* (2011), 1-3, pp. 41-48
[20] Suresh, S., *et al*., Effect of Al_2O_3-Cu/Water Hybrid Nanofluid in Heat Transfer, *Thermal Fluid Science, 38* (2012), Apr., pp. 54-60
[21] Abbasia, S., *et al*., The Effect of Functionalization Method on the Stability and the Thermal Conductivity of Nanofuid Hybrids of Carbon Nanotubes/Gamma Alumina, *Ceramics International*, *39* (2013), 4, pp. 3885-3891
[22] Balla, H., *et al.*, Numerical Study of the Enhancement of Heat Transfer for Hybrid CuO-Cu Nanofluids owing in a Circular Pipe, *Journal of Oleo Science*, *62* (2013), 7, pp. 533-539
[23] Takabi, B., Salehi, S., Augmentation of the Heat Transfer Performance of a Sinusoidal Corrugated Enclosure by Employing Hybrid Nanofluid, *Advances in Mechanical Engineering*, *6* (2014), pp. 1459-1470
[24] Moghadassi, A., *et al.*, A Numerical Study of Water Based Al_2O_3 and Al_2O_3-Cu Hybrid Nanofluid Effect on Forced Convective Heat Transfer, *Int. J. Thermal Science*, *92* (2015), June, pp. 50-57
[25] Wolf-Gladrow, D. A., *Lattice-Gas Cellular Automata and Lattice Boltzmann Models*, Springer, Berlin Heidelberg New York, USA, 2000
[26] Shan, X., Chen, H., Lattice Boltzmann Model for Simulating Flows with Multiple Phases and Components, *Phys. Rev. E.*, *47* (1993), Mar., pp. 1815-1819
[27] Shan, X., Doolen, G., Diffusion in a Multicomponent Lattice Boltzmann Equation Model, *Phys. Rev. E.*, *54* (1996), Oct., pp. 3614-3620

[28] Yang, Z. L., *et al.*, Evaluation of the Darcy's Law Performance for Two-Fluid Hydrodynamics in a Particle Debris Bed Using a Lattice-Boltzmann Model, *Heat Mass Transfer*, *36* (2000), July, pp. 295-304
[29] Zhou, L., *et a.l.*, Multiscale Simulation of Flow and Heat Transfer of Nanofluid with Lattice Boltzmann Method, *Int. J. Multiph. Flow*, *36* (2010), 5, pp. 364-74
[30] Boutra, A., *et al*., Free Convection Heat Transfer of Nanofluids into Cubical Enclosures with a Bottom Heat Source: Lattice Boltzmann Application, Science Direct, *Energy Procsdia*, *139* (2017), Dec., pp. 217-223
[31] Mohebbi, R.., *et al*., Lattice Boltzmann Method Based Study of the Heat Transfer Augmentation Associated with Cu/Water Nanofluid in a Channel with Surface Mounted Blocks, *Int. J. Heat Mass Transfer*, *117* (2018), Feb., pp. 425-435
[32] Izadi, M., *et al*., Numerical Simulation of Natural-convection Heat Transfer Inside a ⊥ Shaped Cavity Filled by a MWCNT-Fe3O4/Water Hybrid Nanofluids Using LBM, Chem. Eng. Proces, *Process Intensif*, *125* (2018), Mar., pp. 56-66
[33] Mohebbi, R., *et al*., Heat Source Location and Natural-Convection in a C-Shaped Enclosure Saturated by a Nanofluid, *Phys. Fluids*, *29* (2017), 122009
[34] Mohebbi, R., *et al*., Lattice Boltzmann Simulation of Nanofluid Natural-Convection Heat Transfer in a Channel with a Sinusoidal Obstacle, *International Journal of Modern Physics*, *29* (2018), 9, 1850079
[35] Mohebbi, R., *et al*., Enhancement of Heat Transfer of Nanofluids in the Presence of Sinusoidal Side Obstacles between Two Parallel Plates Through the Lattice Boltzmann Method, *International Journal of Mechanical Sciences*, *156* (2019), June, pp. 159-169
[36] Frisch, U., *et al*., Lattice-Gas Automata for the Navier-Stokes Equation, *Physical Review Letters*, *56* (1986), 14, pp. 1505-1508
[37] Frisch, U., *et al*., Lattice Gas Hydrodynamics in Two and Three Dimensions, *Complex Systems*, *1* (1987), 4, pp. 649-707
[38] Mohamad, A. A., Applied Lattice Boltzmann Method for Transport Phenomena, Momentum, Heat and Mass Transfer, *The Canadian Jou. of Chemical Engineering, 85* (2007), 6, pp. 946-947
[39] Sidik, N. A. C., Mamat, R., Recent Progress on Lattice Boltzmann Simulation of Nanofluids: A Review, *Int. J. Heat Mass Transfer*, *66* (2015), Aug., pp. 11-22
[40] Khanafer, K., *et al*., Buoyancy-Driven Heat Transfer Enhancement in a 2-D Enclosure Utilizing Nanofluids, *Int. J. Heat Mass Transfer*, *46* (2003), 19, pp 3639-3653
[41] Zou, Q., He, X., On Pressure and Velocity Boundary Conditions for the Lattice Boltzmann BGK Model, *Phys. Fluids*, *9* (1997), 6, pp. 1591-1598
[42] Mohamad, A. A., *Lattice Boltzmann Method,* Springer, New York, USA, 2011
[43] Santra, A. K., *et al*., Study of Heat Transfer due to Laminar Flow of Copper Water Nanofluid through Two Isothermally Heated Parallel Plates, *Int. J. Thermal Sciences*, *48* (2009), 2, pp. 391-400
[44] Bennacer, R., *et al*., Natural-Convection of Nanofluids in a Cavity Including the Soret Effect, *International Journal of Computational Thermal Sciences*, *1* (2009), 4, pp. 425-440

Paper submitted: September 19, 2019
Paper revised: November 24, 2019
Paper accepted: February 18, 2020